



Evidence for the degradation of an emerging pollutant by a mechanism involving iso-energetic charge transfer under visible light

G. Mamba^a, J. Kiwi^{a, **}, C. Pulgarin^a, R. Sanjines^b, S. Giannakis^a, S. Rtimi^{a,c,*}

^a Ecole Polytechnique Fédérale de Lausanne, EPFL-SB-ISIC-GPAO, Station 6, CH-1015, Lausanne, Switzerland

^b Ecole Polytechnique Fédérale de Lausanne, EPFL-SB-IPHY-LPMC, Station 3, CH-1015, Lausanne, Switzerland

^c Ecole Polytechnique Fédérale de Lausanne, EPFL-STI-IMX-LTP, Station 12, CH-1015, Lausanne, Switzerland



ARTICLE INFO

Keywords:

Sputtered ZnO/Cu_xO films
Norfloxacin (NFX) degradation
IFCT
Interface potentials
Catalytic mechanism

ABSTRACT

This study presents the first reports for ZnO/Cu_xO sequentially sputtered leading to stable and uniform films effective accelerated degradation of the emerging pollutant Norfloxacin (NFX) under visible light. The most effective ZnO film was sputtered from a Zn-target for 4 min followed by Cu-sputtering for 30 s on non-thermal resistant polystyrene (PS). The NFX-degradation proceeded more readily on ZnO/Cu_xO compared to ZnO-films although the conduction band potential energy position of the two semiconductors were iso-energetic. By X-ray photoelectron spectroscopy (XPS), Cu₂O was identified as the predominant Cu-oxidation state in the sputtered film. A mechanism for the NFX degradation is suggested in which the holes generated by Cu₂O transfer to ZnO in the ZnO(n)/CuO(p) in the hetero-junction. This transfer is favored by the electrostatic interaction between both semiconductors. The catalyst optical properties and surface potential were monitored during NFX degradation. Stable repetitive NFX degradation kinetics was observed under visible light on the sputtered ZnO/Cu_xO films. The use of appropriate scavengers allowed the identification of the intermediate radical species (ROS). XPS analysis provided the proof for *redox* catalysis taking place within the time of NFX abatement. The application of ZnO/Cu_xO films in a photo-reactor for the degradation of emerging pollutants seems feasible due to the low cost of Zn and Cu and the fast kinetics found for NFX degradation.

1. Introduction

ZnO is a widely used standard photocatalyst in the field of environmental applications [1,2]. It has been used to oxidize a variety of organic pollutants due to the ZnO photo-generated charges under UV band-gap irradiation (only 4–5% of the solar light in the UV-range) [3]. ZnO activity under light is similar or superior to TiO₂. Nevertheless, ZnO is stable in solution at pH > 6.5 and more sensitive to photo-corrosion compared to TiO₂ [4,5]. ZnO is a non-toxic and low-cost material. The optical transitions in ZnO occur with a direct band-gap of 3.3 eV. ZnO is applied in solar cell [6] and as a UV screening agent [7]. ZnO is used in like pigment [8,9], in tire vulcanization [10], CO₂ activation reactions [11], in the production of peroxides [12], in water-splitting activation [13] and in alcohol photo-degradation [14]. The colloidal ZnO formulations/properties have been reported recently by Spanhel et al. [15] and Lingdong et al. [16]. The use of ZnO in the self-cleaning of surfaces under light irradiation has been reported by Bahnenmann et al. [17] and Fallah et al. [18]. The antibacterial properties and performance of ZnO surfaces under light irradiation is a topical

subject gaining increasing attention in the field of photocatalysis as shown by Gedanken et al. [19,20]. ZnO is an inexpensive semi-conducting material used in the electronic industry due to its appreciable electrical conductivity presenting at pH 1 a band-gap (bg) of 3.2–3.4 eV. Depending on nanoparticle size and the preparation method, ZnO presents a conduction band (cb) at 0.1–0.2 V (SHE), a valence band (vb) at ~3.4 (SHE) [21].

All over the world, NFX and related compounds have been detected in surface waters, in ground and drinking water at low concentrations ranging from nano-g L⁻¹ and very seldom up to 1 mg L⁻¹ [22–24]. This fact indicates their ineffective removal from water and wastewater using conventional treatment technologies. This study investigated the removal up to an initial concentration of 20 mg NFX by way of the ZnO/Cu_xO films. The possible detrimental side effects of the presence of fluoroquinolones, NFX and related compounds in the environment are not fully understood but are known to be toxic to plants and aquatic organisms. In 2010, about 120 tons have been reported at a worldwide scale in low concentrations. This stimulates bacterial resistance to antibiotics rendering current antibiotics ineffective in the treatment of

* Corresponding author at: Ecole Polytechnique Fédérale de Lausanne, EPFL-SB-ISIC-GPAO, Station 6, CH-1015, Lausanne, Switzerland.

** Corresponding author.

E-mail addresses: john.kiwi@epfl.ch (J. Kiwi), sami.rtimi@epfl.ch (S. Rtimi).

numerous pathogens. After incomplete removal by conventional wastewater treatment plants, these compounds are found in the sludge, sometimes used as fertilizer, representing an additional input route into the environment. The removal of NFX by biological treatment is ineffective and for this reason, in this study, we address its degradation by way of sputtered films.

The state of the art related to NFX degradation by way of heterogeneous photocatalysis has been reported almost exclusively by way of suspensions and powders [22]. Heterogeneous catalytic/photocatalytic degradation of pollutants require the separation of the catalyst particles from the solution at the end of the NFX degradation cycle. This is expensive in terms of labor, time and chemicals. The same applies if adapted bacterial strains are used in NFX-degradation. TiO_2 suspensions and powders have been recently reported to degrade NFX under light irradiation within 4 h [22–24]. Ding et al. reported magnetite leading to NFX degradation up to 80% [3]. Suspensions of C-TiO_2 have been reported to mineralize 78% of NFX within 70 min [25].

More recently, the NFX degradation by Bi_2WO_6 composites [26] has been reported followed by the study of S. Chen addressing the UV-vis NFX degradation by suspensions of $\text{C/Fe-Bi}_2\text{WO}_6$ [27]. By way of *Bacillus subtilis* adapted bacteria, the NFX-degradation was investigated as a promising approach [28]. However, the degradation needed 26 h and the biofilms handling and preparation was expensive in terms of materials and time leading to a rather slow NFX-biodegradation. Only one report on sol-gel prepared TiO_2 -plates/films degrading NFX under 254 nm light has been reported [29]. Doped ZnO-Cu films prepared by sol-gel annealed at 350 °C on glass have been shown to accelerate the bacterial inactivation under light irradiation [30].

CuO modification to ZnO allows the harvesting of a larger portion of the solar spectrum compared to ZnO . This accelerates NFX degradation. Furthermore, CuOx will inject the photo-generated charges induced by visible light in the ZnO by interfacial charge transfer (IFCT) decreasing the ZnO electron/hole recombination leading to an increase in the lifetime of the photo-generated electron-hole pairs in the ZnO . Evidence is presented in the course of this study for the intermediates and the mechanism leading to the NFX more favorable degradation on $\text{ZnO-Cu}_x\text{O}$ films compared to ZnO films.

The use of supported photocatalysts as suggested in this study has advantages during reactor operation to degrade NFX avoiding: a) the drawback presented by the use of ZnO -suspensions needing separation of the catalyst after each cycle and b) by the use of direct current magnetron sputtering (DCMS) it is possible to deposit uniform, stable and adhesive $\text{ZnO/Cu}_x\text{O}$ films on petri dishes. This avoids the problems inherent to the low temperature film annealing on a substrate leading a lack of mechanical resistance, uniformity and poor adhesion on non-heat resistant substrate [12].

2. Experimental section, materials and methods

2.1. Magnetron sputtering of ZnO/CuOx samples and procedures

The sputtering of petri dishes in reactive atmosphere was carried out by direct current magnetic sputtering chamber (DCMS) as shown in the Supplementary Fig. S1. An AJA vacuum system (AJA International Inc., USA) evacuated the magnetron chamber to 3.5×10^{-6} mbar by a turbo-molecular pump. ZnO was sputtered from a $\text{ZnO-Al}_2\text{O}_3$ (98% ZnO -2% Al_2O_3) target from (Lesker Industries, Hastings Ltd, UK) four inches in diameter and 0.5 in. thick. The added Al_2O_3 to the ZnO -target confers metallic character to the ZnO facilitating the DCMS sputtering from the ZnO -target. The Cu -target used was two inches in diameter, 99.99% pure from the same supplier. The sputtering power was 50 W and the deposition rate 12.5 nm/min as monitored by profilometry (Alphastep500, Tencor, Arizona-USA). The Cu -target was positioned perpendicular to the petri dish at a distance of 10 cm and the petri dishes were rotated during the sputtering at the rate of 20 rpm for 3 min leading to uniform Cu_xO -films. The ZnO film was transparent and

turned orange after Cu-sputtering.

2.2. Total organic carbon determination (TOC), monitoring of the NFX degradation, chemicals and irradiation set-up

The peak of Norfloxacin (molar extinction coefficient $37.500 \text{ M}^{-1} \text{ cm}^{-1}$) during the degradation runs was monitored at 275 nm in a Shimadzu 1800 UV-vis spectrophotometer. The total organic carbon (TOC) was determined in a Shimadzu TOC-500 instrument equipped with an ASI auto-sampler. NaN_3 Fluka was used as singlet oxygen scavenger (${}^1\text{O}_2$), methanol was used as the HO^\cdot -radical scavengers and KI as hole (h^+) scavenger. A concentration of 0.2 mM of scavenger was added in each case to identify each intermediate/radical species. The optical absorption of benzophenone interfering with the absorption of NFX precluded the detection of the superoxide radicals. Volumes of 6 ml were irradiated in the reactor shown in Fig. S2 inside the cavity of a solar simulator. The cavity was provided for with a filter to block UV-light < 310 nm. For the runs monitored in the visible part of the spectrum, a cutoff filter (≤ 410 nm) was used. Norfloxacin solutions were filtered by way of $0.22 \mu\text{m}$ PTFE syringe filter. Samples were equilibrated in the dark for 30 min before the degradation runs. 6 ml NFX solutions in the petri dishes containing 10 mg/l were irradiated in the cavity of a Suntest solar simulator (Heraeus GmbH, Hanau Germany) set at 50 mW/cm^2 or one half of the AM1 value.

2.3. Diffuse reflectance spectroscopy (DRS) and interface potential of the sputtered ZnO/CuOx samples

Diffuse reflectance spectroscopy (DRS) of Cu_xO , ZnO and $\text{ZnO/Cu}_x\text{O}$ sputtered films was carried out a PerkinElmer Lambda 900 UV-vis-NIR spectrometer within the wavelength range of 250–800 nm. Optical spectra were analyzed by the Tauc's method. Some semiconductors present both, direct and indirect inter-band transitions. The direct band gap is common on thin films, whereas indirect band-gap transitions are generally found for relatively thick films. For indirect transitions, the Tauc's relations can be written as:

$$\alpha = \frac{B}{h\nu} (h\nu - E_g)^2 \quad (1)$$

where: B is the Tauc constant, $h\nu$ is related to the photon energy, E_g is the optical band-gap of the material, α is the absorption coefficient extracted from the transmittance (T) and reflectance (R) measurements for the sample using the equation:

$$\alpha = \frac{1}{d} \ln \frac{T_Q(1 - R_s)}{T_s} \quad (2)$$

where: d is the thickness of the film; Q and S refer to quartz or the sample, respectively. Tauc's treatment of the data holds for $\alpha > 10^4 \text{ cm}^{-1}$.

The indirect transition is obtained by plotting $(\alpha \times h\nu)^{1/2}$ versus $h\nu$. E_g corresponds to the intercept of the linear fit with the abscissa. The direct transition is obtained by plotting $(\alpha \times h\nu)^2$ versus $h\nu$.

The sample local pH and interfacial potentials were monitored by means of a Jenco 6230 N (pH/mV/temperature meter) with a hand-held microprocessor in splash proof case with a 3 points calibration. The signals were monitored via RS-232-C IBM compatible communication interface and BNC, pH/ORP DIN ATC connector. The electrode was contacted with the sample and the measurements were taken after a suitable delay required for the sample stabilization. The redox/pH electrode was standardized using two redox solutions (240 mV and 470 mV; Hanna Instruments, Switzerland) and three pH standards. After each analysis, the electrode was kept in a mixture (70% v/v) of distilled water and ethyl alcohol for 16 h. Before each experiment, the electrodes were washed with MQ-water. After use, it is necessary to polish it with a fine alumina oxide powder (Sigma Aldrich, Switzerland) to restore the electrode platinum surface.

2.4. X-ray photoelectron spectroscopy (XPS) of the samples during NFX degradation

An AXIS NOVA photoelectron spectrometer (Kratos Analytical, Manchester, UK) was used for the XPS measurements equipped with a monochromatic AlK α ($\hbar\nu = 1486.6$ eV) anode. The carbon C1s line with position at 284.6 eV was used as a reference to correct for the charging effects. Known sensitivity factors for each element were used to report the composition of the films upper layers < 10 nm [32,33]. The deconvolution of the XPS-peaks was processed in a CasaXPS-Vision 2, from Kratos Analytical (UK) taking into consideration the Shirley correction for charging effects [34]. Changes in CuO/Cu_xO surface atomic concentration percentage ratio in the ZnO(4 min)/Cu_xO(30 s) film were determined by XPS before and after NFX degradation.

2.5. Coatings characterization: atomic force microscopy (AFM) and X-ray diffraction (XRD)

The crystallography of the ZnO/Cu_xO films was determined by X-ray diffraction (XRD) using Cu K α radiation at a grazing incident angle of 4° (XPert MPD PRO from PANalytical). The topography of the films was registered by atomic force microscopy (AFM) in a PSIA (Xe-100) instrument in non-contact mode.

3. Results and discussion

3.1. Effect of the sputtering time of ZnO/Cu_xO on the NFX degradation and TOC-reduction

Fig. 1a presents the reduction of the NFX concentration on sputtered ZnO/Cu_xO at different times when irradiated under solar simulated light at pH 6.5 since ZnO has been reported to be stable in solution \geq pH 6.5 [35]. The reduction of the total organic carbon (TOC) on ZnO, Cu_xO and the optimized ZnO (4 min)/Cu_xO (30 s) sample are presented in Fig. 1b. The TNFX irradiation was carried out in the experimental set-up shown in Fig. S2, supplementary material. By inspection of the data presented in Fig. 1 and Supplementary Figs. S3 and S4, NFX degradation mediated by ZnO and Cu_xO led to a slower kinetics compared to the NFX degradation mediated by ZnO (4 min)/Cu_xO(30 s). Fig. 1, trace 1) also shows a slow degradation in the dark due to Cu [20]. The effect of the initial concentration of NFX on the degradation kinetics mediated by the ZnO(4 min)/Cu_xO(30 s) sample is presented in the supplementary Fig. S5. The data shown in Fig. 1a suggests that the effect of the Cu_xO in the composite ZnO/Cu_xO film: a) increases the charge carrier lifetime compared to ZnO films, b) acts a recombination center for the charges generated in the ZnO and c) reduce the ZnO over-potential required for the NFX degradation. The error bars represent the standard deviation at $n = 5\%$.

3.2. Semiconductor behavior of ZnO/Cu_xO films leading to NFX degradation: differentiated effects of visible and solar light and catalyst recycling

Degradation of NFX on ZnO/Cu_xO occurs to a small extent in the dark and to a large extent under light (see Fig. 2a). Fig. 2a, trace 1) shows the degradation in the dark catalyzed by the (4 min)/Cu_xO (30 s) sample. Cu-ions leaching from the sample surface may induce NFX-degradation. But a very low leaching of copper during NFX degradation on Cu-sputtered petri dishes was reported recently by Mamba et al. [41] reporting amounts of ~ 1 ppb.

Fig. 2a shows that as the applied light dose increased, the degradation kinetics becomes faster. A bigger amount of photo-generated charges by the ZnO (4 min)/Cu_xO(30 s) at higher light doses lead to a faster NFX degradation. Intermediate-radical species leading to NFX degradation will be addressed below in Section 3.5. The effects of visible light irradiation > 410 nm compared to the solar light > 310

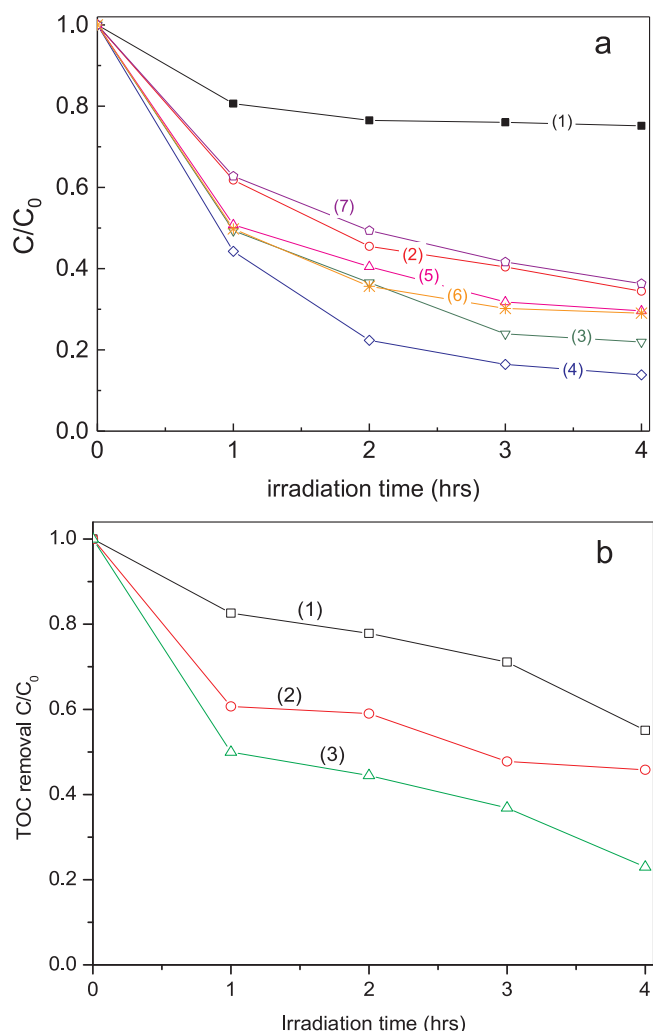


Fig. 1. (a) Effect of Cu_xO sputtering deposition time of ZnO/Cu_xO on Norfloxacin (NFX) reduction: (1) ZnO(4 min)/Cu_xO(30 s) in the dark, Light activated reactions: (2) ZnO(4 min)/Cu_xO(10 s), (3) ZnO(4 min)/Cu_xO(20 s), (4) ZnO(4 min)/Cu_xO(30 s), (5) ZnO(4 min)/Cu_xO(60 s), (6) ZnO (4 min) and (7) Cu_xO (30 s). The initial pH 6.5, [NFX] = 10 mg/L, light intensity: 50 mW/cm²). For more details see text. (b) TOC removal over: (1) ZnO(4 min), (2) Cu_xO(30 s) and ZnO(4 min)/Cu_xO(30 s). (Initial pH 6.5, [NFX] = 10 mg/L, light intensity: 50 mW/cm²).

nm on the NFX degradation are shown in Fig. 2b. The visible light dose was 35 mW/cm² vs. 50 mW/cm² for the solar simulated light when no filter was used.

The stable repetitive NFX-photo-degradation on ZnO (4 min)/Cu_xO (30 s) samples is shown in Fig. 3. The decrease in the repetitive degradation kinetics in Fig. 3 was due to residual fragments of the NFX remaining/accumulated on the sample surface.

3.3. Diffuse reflectance spectroscopy (DRS) and changes of pH and interface potential during NFX degradation

Fig. 4 shows the DRS spectra of Cu_xO, ZnO/Cu_xO and ZnO films on Petri dishes. The rough surface of the sputtered Petri dishes does not allow the UV-vis reflectance data to be used directly to assess the absorption coefficient of the sputtered films shown in Fig. 4 due to the large scattering contribution in the reflectance spectra. Normally a weak dependence is assumed for the scattering coefficient S on the wavelength. Therefore, the DRS data is plotted in Kubelka-Munk (KM)

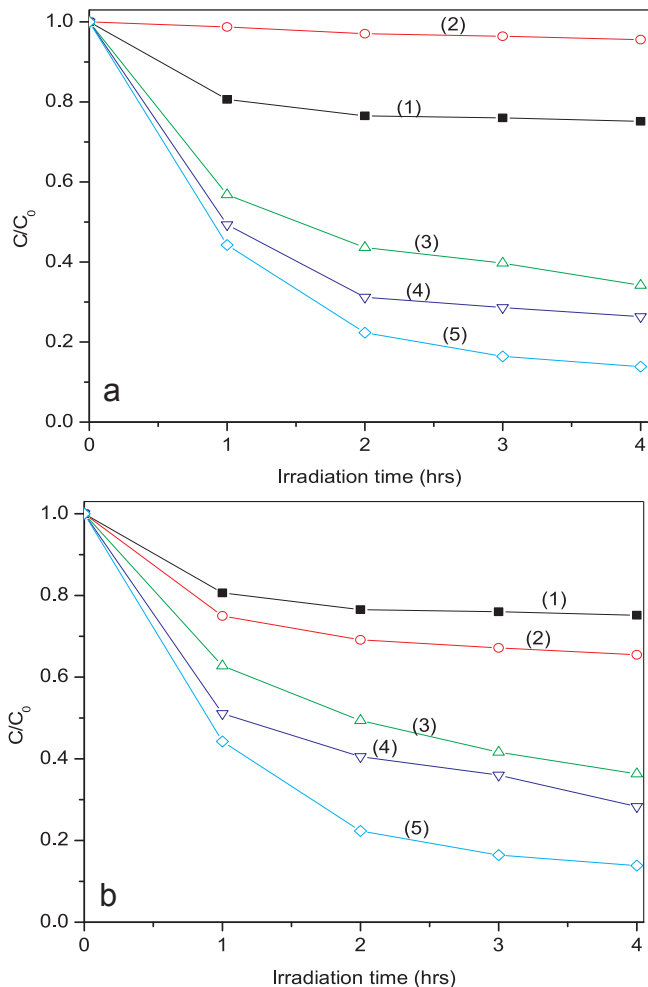


Fig. 2. (a) Effect of light intensity on NFX degradation over ZnO(4 min)/Cu_xO(30 s): (1) dark runs (2) Petri dish alone irradiated under 50 mW/cm², (3) under light 15 mW/cm², (4) under light 30 mW/cm² and (5) under light 50 mW/cm². (Initial pH 6.5, [NFX] = 10 mg/L). (b) Effect of the light source on NFX degradation (1) ZnO(4 min)/Cu_xO(30 s) in the dark, (2) ZnO(4 min) under visible light > 400 nm, (3) ZnO(4 min) under solar simulated light in the range 310–800 nm, (4) ZnO(4 min)/Cu_xO(30 s) under visible light only and (5) ZnO(4 min)/Cu_xO(30 s) under solar simulated light (Initial pH 6.5, [NFX] 10 mg/L, light intensity 50 mW/cm²).

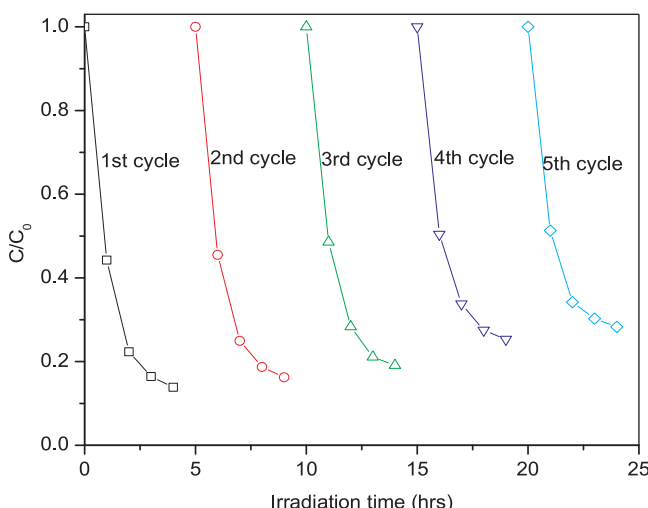


Fig. 3. Reuse of the ZnO(4 min)/Cu_xO(30 s) film over five cycles (initial pH 6.5, [NFX] 10 mg/L, light intensity 50 mW/cm²).

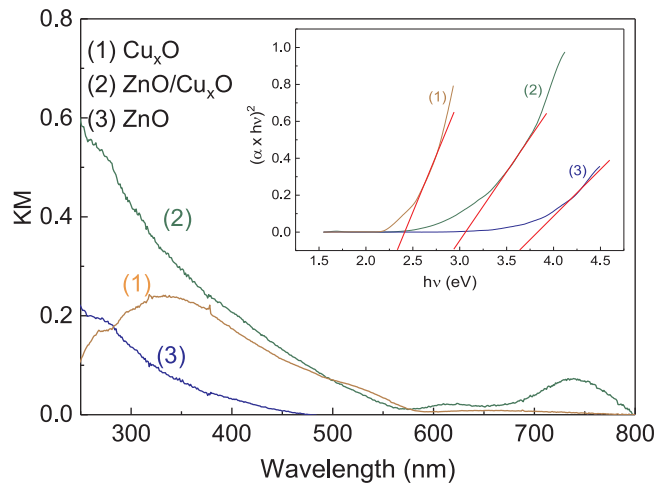


Fig. 4. Diffuse reflectance spectroscopy (DRS) of Cu_xO (30 s), ZnO (4 min) and ZnO/Cu_xO (4 min/30 s) sputtered Petri dishes. The insert shows the Kubelka-Munk plot for Cu_xO, ZnO/Cu_xO and ZnO leading to the determination of the band-gaps. For other details, see text.

units following Tauc's method [36]. The optical band-gap for each catalyst was estimated extrapolating the linear part of the spectra in the insert in Fig. 4 vs the energy axis in eV units. The insert in Fig. 4, trace (1), shows a band-gap (bg) ~ 2.35 eV for the Cu_xO. This shows that the film consists of CuO and Cu₂O [12]. For the ZnO/Cu_xO film, a bg ~ 2.9 eV was found as shown by the insert in Fig. 4 shows a narrowing of the band gap of ZnO (3.20–3.40) eV due to the added Cu_xO [31]. The higher optical absorption by ZnO/Cu_xO films in Fig. 4 leads to a formation of a higher amount of photo-generated charges with respect to ZnO alone. This induces a faster NFX degradation kinetics by ZnO/Cu_xO compared to ZnO and Cu_xO films (see Fig. 1a).

The surface potential for the Cu_xO during NFX degradation up to 400 min was also investigated to gain insight into the mechanism of NFX inactivation and the data obtained is presented in Fig. S6. The interfacial surface potential or Eigenvalue or initial potential surface decreases from 210 mV to 130 mV within 80 min during the NFX degradation. This is due to the variation in the interfacial contact occurring during NFX degradation. A pH-decrease from 6.80 down to 6.35 was also observed during the degradation of NFX as shown in the right-hand side in Fig. S6-a. This is equivalent to about a five-fold increase in the concentrations of [H⁺]. The concomitant decrease observed in the pH is due to the production of short-chain carboxylic acids (C1–C4) with pK_a values around ~ 3.0 [12,23]. These carboxylic acids are subsequently eliminated during NFX mineralization (see Fig. 1b) by way of the photo-Kolbe reaction [37]:



This explains the recovery of the pH to values > 6.7 once the carboxylic acids/CO₂ are eliminated from the solution. Norfloxacin is present in the solution as an NFX-anion at pH > 6.30 . This enhances the electrostatic interaction of the NFX with the slightly positively charged Cu_xO [24,25]. Fig. S6-b the initial Eigenvalue interfacial for the ZnO/Cu_xO surface lies potential is 60 mV lower when compared with the value found for Cu_xO in. This reveal a significant change in the surface energetics compared to the value found for the Cu_xO-films. The time of NFX degradation decreases to ~ 50 min, a shorter time compared to the Cu_xO-films. Finally, Fig. S6-c reports the complicated trend for the surface potential changes of ZnO during NFX degradation showing a lower decrease in the surface potential. This may explain the slower NFX degradation kinetics induced by ZnO in Fig. 1a compared to the degradation mediated by Cu_xO and/or ZnO/Cu_xO.

3.4. XPS determination of ZnO , Cu_xO and ZnO (4 min)/ Cu_xO (30 s) samples during NFX degradation: evidence for redox processes

Table 2 presents the data for the deconvoluted XPS peaks of $\text{Cu}2p$ and $\text{O}1s$ obtained from the sample ZnO (4 min)/ Cu_xO (30 s) before and after NFX degradation. The $\text{Cu}2p3/2$ peaks were deconvoluted at times zero and after four hours reaction. The binding energy (BE) of Cu_2O ($\text{Cu}2p3/2$) is 932.1 eV and shifts to 932.5 eV after NFX degradation. A higher binding energy (BE) means a higher oxidized Cu_xO . This shift in the XPS spectrum provides the evidence for redox catalysis taking place in the Cu_xO during NFX degradation. A BE shift ≥ 0.2 eV is generally associated with the appearance of a new species [33]. The term Cu_xO has been used repeatedly in this study. This is justified by the fact that DCMS-sputtering deposits simultaneously Cu_2O and CuO on the ZnO petri dishes. The Cu-oxide ratio is dependent on the experimental conditions during petri dish sputtering. The $\text{CuO}(\text{Cu}2p1/2)$ peak at time zero of 934.5 eV in shifts after 4 h to a BE 934.9 eV as shown in **Table 2**. Peaks shift of $\text{Zn}2p$ before and after NFX degradation is shown in supplementary Fig. S7.

The percentage area of Cu_2O increased by about 30% after 4 h during NFX-degradation, while the CuO surface area decreased by a lower percentage. Practically no redox shifts for the $\text{Zn}2p$ samples was observed within the 4 h NFX degradation time (see Supplementary Fig. S7). This is due to the high stability of Zn, the element number 30 of the periodic system. The negatively charged electrons in the Zn reside in orbitals close to the positively charged atomic nucleus leaving the un-filled orbitals 3d4s. This generates a high electrostatic attraction between the Zn-electronic cloud and the atomic nucleus inducing higher energies in the Zn to participate in chemical reactions. The $\text{O}1s$ peak of ZnO (see supplementary materials S7) was deconvoluted into two peaks, namely O1 and O2. The O2 peak is associated with O^{2-} ions in oxygen deficient regions within the matrix of the ZnO (especially $\text{Zn}-\text{OH}$) and these regions are related to oxygen defects in the sputtered thin film. The Zn(I)(3d¹⁰ 4s²) and Zn(II)(3d¹⁰ 4s¹) oxidation states require much higher potentials compared to Cu(I)/Cu(II) to intervene in chemical reactions or reduction/oxidation processes. In the case of Cu (element number 29) the electronic cloud is not closely packed around the positive atomic nucleus leaving negatively charged electrons free to react. **Table 1**, shows the values for the surface percentage atomic composition at time zero for Cu_2O and CuO respectively of 48% and 52%. The Cu_2O percentage increases to 62% during the 4 h NFX degradation becoming the main component in the Cu_xO sample. This information is used in Section 3.6 when suggesting the composition of the ZnO (4 min)/ Cu_xO (30 s) sample as made up predominantly by Cu_2O / ZnO (see hetero-junction scheme in Fig. 6a).

Supplementary Fig. S8 a–c) shows the Auger and photoelectron line energies for ZnO , Cu_xO and $\text{Cu}_x\text{O}/\text{ZnO}$ respectively. The Zn(LMM) peaks before and after NFX degradation in Fig. S8a–c) show insignificant changes of the topmost sample layers. However, considerable shifts of the Auger and photoelectron line energies were observed for the Cu lines after NFX degradation. Moreover, in the composite $\text{ZnO}/\text{Cu}_x\text{O}$ film, some Zn-peaks were not seen in the 9c survey spectra. This is due to the screening effect of the Cu upper layers hindering the appearance of the signals from the Zn under-layers.

Table 1
Changes in $\text{CuO}/\text{Cu}_2\text{O}$ surface percentage ratio in ZnO (4 min)/ Cu_xO (30 s) measured by XPS before and after NFX degradation.

Sample	% Cu_2O	% CuO
Unused ZnO (4) Cu_xO (30) (at time zero)	48	52
Used ZnO (4) Cu_xO (30) (after 4 h)	62	38

Table 2

XPS deconvolution of $\text{Cu}2p$ and $\text{O}1s$ from ZnO (4 min)/ Cu_xO (30 s) before and after NFX degradation.

	Species	Binding Energy (BD) before NFX degradation (4 h)	Binding Energy(BE) after NFX degradation(4 h)
ZnO(4 min)/ Cu_xO (30 s)	$\text{Cu}2p$	Cu_2O at 932.1 eV CuO at 934.5 eV	Cu_2O at 932.5 eV CuO at 934.9 eV
	$\text{Cu}2p1/2$	Cu_2O at 952.3 eV CuO at 954.6 eV	Cu_2O at 952.3 eV CuO at 954.4 eV
	Satellite	940 eV, 944 eV, 962 eV	942 eV, 944 eV, 963 eV
	$\text{O}1s$	529.9 eV	530.5 eV
	O1	531.1 eV	531.7 eV
	O2		

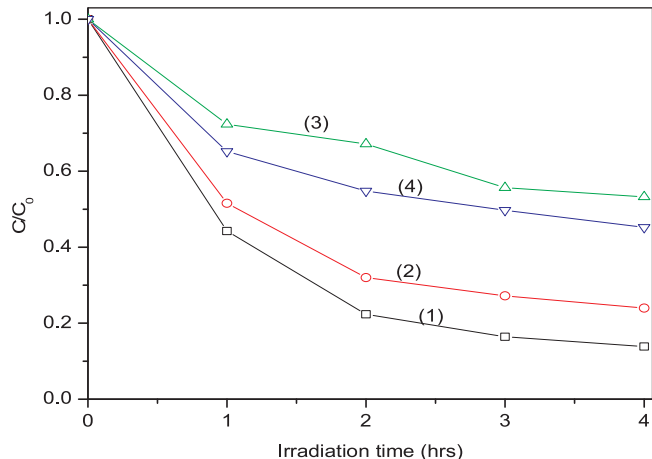
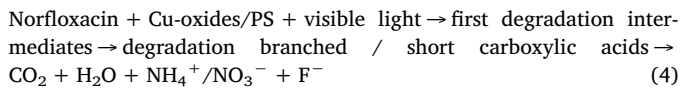


Fig. 5. Effect of the addition of different radical scavengers on the NFX degradation over ZnO (4 min)/ Cu_xO (30 s) : (1) No scavenger, (2) adding NaN_3 , (3) adding KI and (4) adding CH_3OH . Initial pH 6.5, [NFX] 10 mg/L, light intensity 50 mW/cm².

3.5. Scavenging of the radicals leading to NFX degradation: unambiguous identification of the intermediated reactive oxidative species

The oxidative radical intermediates during NFX-oxidation were monitored for the ZnO (4 min)/ Cu_xO (30 s) sample and the results shown in **Fig. 5**. The quenching of the intermediate radicals was seen to proceed more readily compared to the scavenging experiments on ZnO and Cu_xO by themselves reported in supplementary Figs. S9 and S10. The radical scavengers used were sodium azide (NaN_3) for a singlet oxygen (${}^1\text{O}_2$), methanol for hydroxyl radical (HO^\cdot), (KI) for the $\text{vb}(\text{h}^+)$ and benzoquinone for the superoxide radicals [37]. A concentration of 0.2 mM of scavenger was added in each case to identify each intermediate/radical species. The optical absorption of benzophenone and Norfloxacin precluded the detection of the superoxide radicals. **Fig. 5** shows that the $\text{CuOvb}(\text{h}^+)$ holes were the most important species leading to Norfloxacin degradation. The overall reaction leading to NFX degradation can be written as:



The unambiguously determination by NaN_3 to quantify the effect of ${}^1\text{O}_2$ and the use of CH_3OH to quantify HO^\cdot radical-scavengers is not possible. NaN_3 is also an HO^\cdot radical scavenger and possibly ${}^1\text{O}_2$ and HO^\cdot intervene jointly in the Norfloxacin oxidation. **Fig. 5** shows that the HO^\cdot radical ($\text{OH}^\cdot/\text{HO}^-$ – 1.90 V vs NHE) [37] intervenes more readily in NFX oxidation compared to ${}^1\text{O}_2$ singlet due to the lower potential reported for the O_2/O_2^- reaction of –0.16 V SCE [38–40]. The experiments leading to the identification of the intermediate

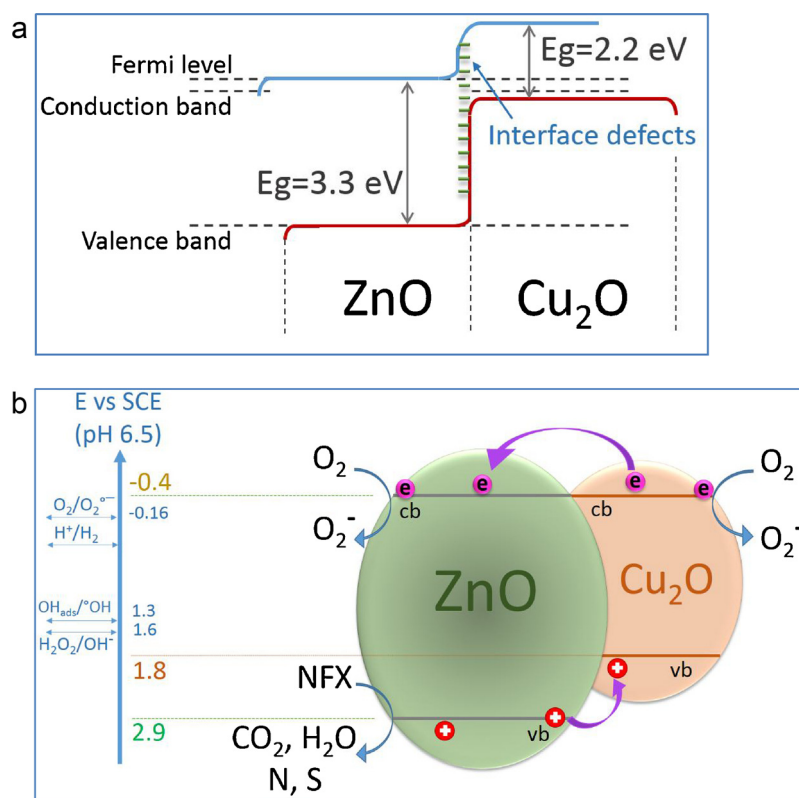


Fig. 6. (a) Suggested position for the energy bands at the ZnO/Cu₂O hetero-junction. (b) Mechanism suggested for the interfacial charge transfer (IFCT) between ZnO and Cu₂O with potential energy bands position at pH 6.5.

radicals have been interpreted using the conventional framework of the radical-species photo-generated during the TiO₂ photocatalysis [12,40]. Cu-oxide do not necessarily follow the same pattern hold for the generation of radical species mediated by ZnO/Cu_xO during NFX photodegradation.

3.6. Suggested reaction mechanism and interfacial charge transfer (IFCT) in ZnO/Cu_xO under solar light Irradiation

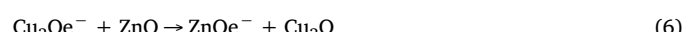
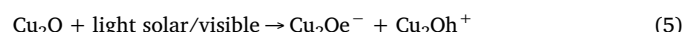
The degradation of a pollutant in solution is a carried out at a certain pH. The solution pH determines the dissociation of the pollutant in the solution. The initial NFX pH was 6.5 and this is higher than the pK_a of NFX of 6.1 [38]. The NFX is therefore present in solution mainly in the anionic form. ZnO has been reported with an isoelectric point (I.E.P.) between 8.0 and 10.3 depending on the variety of ZnO used [39,40]. The NFX-anion will be preferentially adsorbed on the ZnOH₂⁺ present at pH 6.5. Due to electrostatic attraction with the negatively charged NFX, the pH of the solution during NFX degradation dropped from 6.5 to 6.0 (see Figs. 1 and 2).

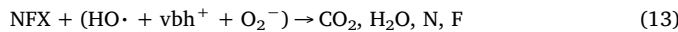
In the ZnO/CuO hetero-junction presented in Fig. 6a, the equilibration between the Cu₂O/ZnO photo-generated electrons and holes in the Fermi level involve charge compensation when ZnO and Cu₂O reach thermal equilibrium [40]. Cu₂O was found by XPS (Section 3.4) to be the majority oxide as shown in Table 1 and this is the reason to include this oxide in the scheme for the ZnO/CuO hetero-junction suggested in Fig. 6a. The positive holes generated by Cu₂O reach the ZnO depletion layer and hinder recombination accelerating the NFX degradation. The ZnO doping by Cu has several effects on the photocatalysis of ZnO: a) It changes the electronic structure of the ZnO resulting in changes in the position of the ZnO Fermi level, b) it leads to the formation of new electronic levels due to the interaction of the Cu with the ZnO as discussed above in Section 3.4, c) it increases the electron conductivity of ZnO due to the added Cu/CuO, d) it modifies the ZnO surface properties/sites active in photocatalytic processes and finally e) it red-shifts

the absorption edge of ZnO due to electrons jumping from the ZnOvb to the ZnOcb. We have reported recently the degradation of NFX on CuO sputtered films but in this case the photocatalyst consisted of Cu₂O(p) and the CuO(n) species [41]. A different type of p-n coupling takes place in the ZnO/CuO heterojunction compared to the case of the CuO(p)CuO(n) interaction (Fig. 6a).

Fig. 6b suggests a scheme for the interfacial charge transfer (IFCT) from Cu₂O to ZnO samples at pH 6.5 vs SCE under solar/visible light irradiation [21,40–43]. The iso-energetic electron transfer refers to the effective transfer of the cb- from Cu₂O to ZnO. This was not expected *a priori* since the cb of Cu₂O and ZnO are practically at the same potential energy level. Generally, the interfacial charge transfer is triggered and accelerated by the difference of the cb position of the two particles involved in the transfer process. But during the course of the present study a considerably acceleration of the NFX degradation was observed in Figs. 1 and 2 when Cu₂O was sputtered in small amounts on the ZnO-film. This was unexpected in view of the iso-energetic nature of the electron transfer shown schematically in Fig. 6b.

The study presents the first evidence for the iso-energetic charge transfer between Cu₂O and ZnO as described by Eq. (5). In addition, the p-type Cu₂O interacts electrostatically with ZnO favoring further the electron transfer to the ZnO n-type semiconductor in Fig. 6a and b. The degradation of NFX can be suggested as proceeding Eqs. (4)–(12).





The conduction bands of Cu_2O and ZnO in Fig. 6b are seen to be more negative relative to the standard O_2/O_2^- potential of -0.16 V vs SCE [40]. The ZnO VB potential is energetically in a position to produce the $\text{HO}\cdot$ -radicals able to degrade NFX as noted by the VB of ZnO (Fig. 6b). The potentials for the Eqs. (4)–(12) have been reported in references [31–40,41] but the combined potentials of the individual reactions is not known. This combined potential is the one determining the kinetics of the process leading to NFX degradation. However, the potential of the combined set of reactions is difficult to determine. Cu_2O (Cu^+ in net sense) is a deep trap for electrons as noted above in Eqs. (4)–(5). The charge injection from Cu_2O to ZnO is not only important in processes related to the degradation of emerging pollutants but has been reported for CuO/ZnO in gas sensors [44], photocatalytic production of H_2 [45] and core shell $\text{ZnO}/\text{Cu}_2\text{O}$ nano-composites reacting with dyes [46,47].

3.7. Atomic force microscopy (AFM) and X-ray diffraction (XRD) of ZnO and $\text{ZnO}/\text{Cu}_x\text{O}$ films

Fig. 7 presents the AFM data for ZnO and $\text{ZnO}/\text{Cu}_x\text{O}$ sputtered on non-porous/flat SiO_2 wafers to avoid the petri dish porosity. The mean average surface roughness value found was of $\text{Rg} \geq 12.4$ nm for ZnO and $\text{Rg} \geq 19.8$ nm, both values in the range of smooth surfaces. The mean average roughness (Rg) is the arithmetic average of the vertical

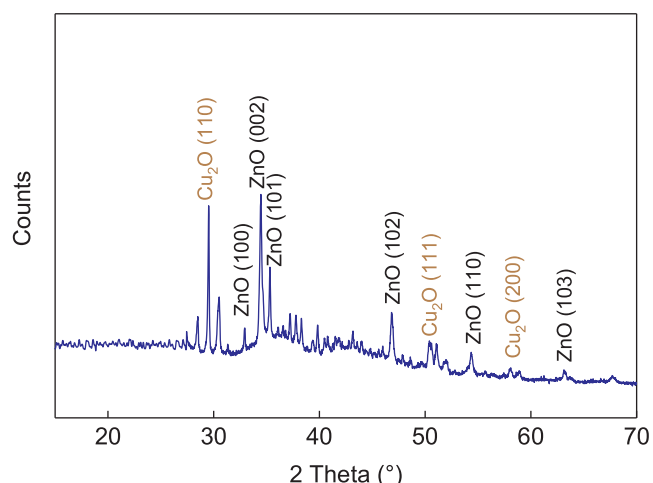


Fig. 8. X-ray diffraction (XRD) data obtained for the optimized film of $\text{ZnO}/\text{Cu}_x\text{O}$ sputtered for 4 min/30 s leading to fast NFX degradation.

deviations from the central plane surface. AFM provides accurate values for Rg in the nanometer scale. Fig. 7a shows the AFM images of ZnO samples sputtered for 4 min and the AFM images for the $\text{ZnO}/\text{Cu}_x\text{O}$ samples sputtered for 4 min/30 s respectively in a scanned area of $300 \times 300 \mu\text{m}^2$. Taking the Norfloxacin size of about 6–10 nm [38], the interaction of Norfloxacin with both sputtered film is due to: a) the capillary forces between Norfloxacin and the Cu_xO , b) to electrostatic

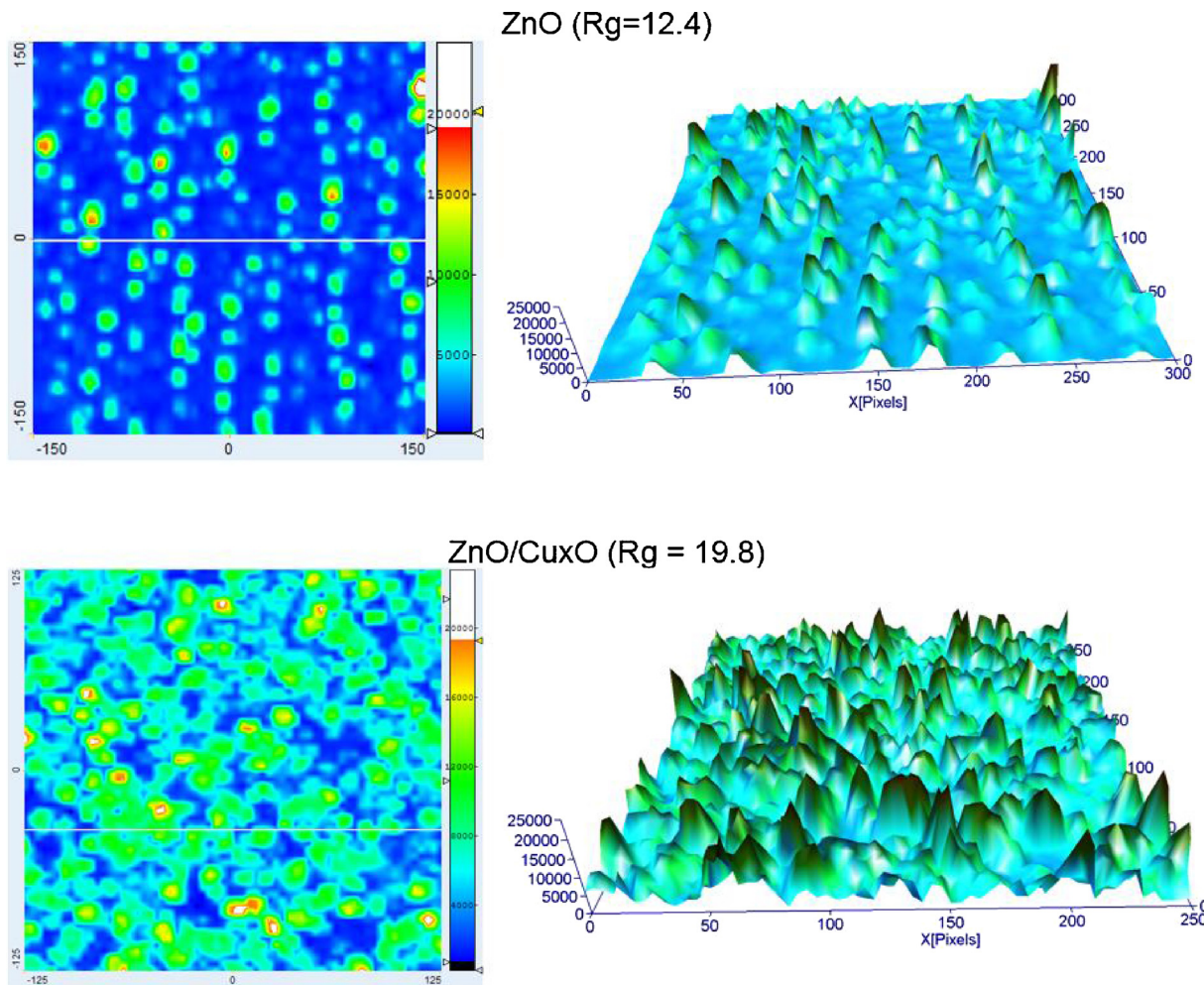


Fig. 7. AFM imaging of a) ZnO ($\text{Rg} = 12.4$) and b) $\text{ZnO}/\text{Cu}_x\text{O}$ ($\text{Rg} = 19.8$) on Si-wafer sputtered for 4 min and 4 min/30 s respectively. For more details, see text.

effects, c) to van der Waals forces, d) to the oxydo-reduction potentials and finally e) to the hydrophobic/hydrophilic interactions between Norfloxacin and the ZnO and/or ZnO/Cu_xO surfaces shown in Fig. 7. The capillary forces reaching the interstitial NFX by higher pillars in ZnO/Cu_xO compared ZnO lead to a faster catalytic degradation of NFX.

Fig. 8 presents the X-ray diffraction (XRD) spectrum of the optimized ZnO/Cu_xO film leading to NFX degradation (see in Fig. 1, trace 4). The intensity of the diffraction lines depends on the cluster growing process as well as the deposition conditions. The X-ray diffraction lines reflect the various degrees of crystallinity for ZnO and Cu₂O on the films. The sharp narrow peaks found for ZnO and Cu₂O in Fig. 8 are assigned to well crystallized ZnO and Cu₂O oxides. The frequency of the Cu-signals in Fig. 8 is substantially lower compared to the ZnO signals. This is expected from the small amount of Cu present in the ZnO/Cu_xO film. The most prominent atomic plane for Cu was the Cu₂O (110) plane. The Cu₂O (111) smaller peak is seen in Fig. 8 along the Cu (200) peak. The average grain sizes for the Cu₂O was estimated by the Scherer's equation of ~24 nm. The most prominent peak for ZnO(002) vertical to the petri dish plane reflects the preferred growth orientation for the ZnO atomic planes [48]. Cu_xO peak phases have been reported at 33.1° and 35.8° and 38.7° in agreement with the standard reference JCPDS #05-0661 [49]. The CuO peak appears practically at the same position of the X-ray diffraction ZnO (002) peak in Fig. 8 [48,49]. Small amounts of Cu in the ZnO crystallographic structure share the O of the ZnO improving the ZnO (002) peak size [49]. Any shift in the ZnO (002) peak due to the Cu-doping is beyond the resolution of the X-ray spectrogram in Fig. 8. Some work has claimed that the ZnO peak positions is shifted upon Cu-addition to higher 2θ-values, which is indicative of a contraction in the ZnO-unit cell. This is also beyond the resolution limit of the X-ray data reported in Fig. 8 [47–50] and needs deeper investigation.

4. Conclusions

The contamination of water bodies by furtive emissions like NFX is a worldwide problem. The degradation of NFX requires at the present time the development of more advanced catalyst/photocatalyst showing an improved kinetics and stability leading to longer operational lifetimes. The supported catalysts developed present a potential application in the environmental field to degrade recalcitrant pollutants in reactors during long operational times. This study presents the first report on ZnO/Cu_xO films sputtered on low thermal resistant like polystyrene (PS) petri dishes leading to NFX photo-degradation under visible/solar irradiation. It was found that iso-energetic processes occur between Cu₂O and ZnO leading to NFX degradation under visible light irradiation. The radicals generated during NFX degradation were identified by appropriate scavenging experiments. By XPS, the presence of Cu₂O was identified as the predominant Cu-oxide present in the films. A mechanism is suggested by which Cu₂O^{h+} holes transfer charge to ZnO in an iso-energetic process. XPS changes on the film surface Cu-oxidation states provided the evidence for *redox* processes on the ZnO/Cu_xO film during the NFX degradation process.

Acknowledgments

We thank the EPFL financial supports and the Swiss government excellence scholarship for the post-doctoral fellowship of Gcina Mamba at the EPFL, Lausanne, Switzerland.

Appendix A. Supplementary data

Supplementary material related to this article can be found, in the online version, at doi:<https://doi.org/10.1016/j.apcatb.2018.03.109>.

References

- [1] A. McLaren, T. Valdes-Solis, G. Li, S. Tsang, Shape and size effects of ZnO nanocrystals on photocatalytic activity, *J. Am. Chem. Soc.* 35 (2009) 12540–12541.
- [2] X. Bai, L. Wang, R. Zong, Y. Lu, Y. Sun, Y. Zhu, Performance enhancement of ZnO photocatalyst via synergic effect of surface oxygen defect and graphene hybridization, *Langmuir* 29 (2013) 3097–3115.
- [3] R. Georgekutty, M. Seery, S.C. Pillai, A highly efficient Ag-ZnO photocatalyst: synthesis, properties, and mechanism, *J. Phys. Chem. C* 112 (2008) 13563–13570.
- [4] S. Girish Kumar, K.S. Koteswara Rao, Zinc oxide based photocatalysis: tailoring surface-bulk structure and related interfacial charge carrier dynamics for better environmental applications, *RSC Adv.* 5 (2015) 3306–3351.
- [5] A. Iglesias-Juez, F. Vines, O. Lamiel-Garcia, M. Fernandez Garcia, F. Illas, Morphology effects in photoactive ZnO nanostructures: photo-oxidative activity of polar surfaces, *J. Mater. Chem. A* 3 (2015) 8782–8792.
- [6] C. Karunakaran, V. Rajeswari, P. Gomathisankar, Enhanced photocatalytic and antibacterial activities of sol-gel synthesized ZnO and Ag-ZnO, *Mater. Sci. Semicond. Process.* 14 (2011) 133–138.
- [7] S. Ansari, M. Khan, S. Kalathil, A. Nisar, J. Lee, M. Cho, Oxygen vacancy induced band gap narrowing of ZnO nanostructures by an electrochemically active biofilm, *Nanoscale* 5 (2013) 9238–9246.
- [8] A. Mozezi, A. McDonagh, M. Cortie, Zinc oxide particles: synthesis, properties and applications, *Chem. Eng. J.* 185–186 (2012) 1–22.
- [9] C. Auer, W. Griebel, B. Jahn, *Industrial Inorganic Pigments*, Wiley Verlag, Weinheim, 2005.
- [10] P. Nieuwenhuizen, Zinc accelerator complexes: versatile homogeneous catalysts in sulfur vulcanization, *Appl. Catal. A* 207 (2001) 55–68.
- [11] Y. Wang, R. Kovacic, B. Meyer, K. Kotsis, D. Stodt, V. Stamm, H. Qiu, F. Trager, D. Langenberg, M. Muhlerand, C. Woll, Tuning the reactivity of oxide surfaces by charge-accepting adsorbates, *Angew. Chem. Int. Ed.* 46 (2007) 7315–7318.
- [12] C. Kormann, D.W. Bahnemann, M.R. Hoffmann, Photocatalytic production of hydrogen peroxides and organic peroxides in aqueous suspensions of titanium dioxide, zinc oxide, and desert sand, *Environ. Sci. Technol.* 22 (1988) 798–806.
- [13] K. Maeda, K. Domen, Solid solution of GaN and ZnO as a stable photocatalyst for overall water splitting under visible light, *Chem. Mater.* 22 (2010) 612–623.
- [14] L. Xu, Y.L. Hu, C. Pelligra, C.H. Chen, L. Jin, H. Huang, S. Sithambaram, M. Aindow, R. Joosten, S.L. Suib, ZnO with different morphologies synthesized by solvothermal methods for enhanced photocatalytic activity, *Chem. Mater.* 21 (2009) 2875–2885.
- [15] L. Spanhel, Colloidal ZnO nanostructures and functional coatings: a survey, *J. Sol-Gel Sci. Technol.* 39 (2006) 7–24.
- [16] J.Z. Lingdong, J. Huilan, Ch. Chunchua, Control of ZnO morphology via a simple solution route, *Chem. Mater.* 14 (2002) 4172–4177.
- [17] R. Fateh, R. Dillert, D. Bahnemann, Self-cleaning properties, mechanical stability, and adhesion strength of transparent photocatalytic TiO₂-ZnO coatings on polycarbonate, *ACS Appl. Mater. Interfaces* 6 (2014) 2270–2278.
- [18] H. Fallah, A. Shojaei, M. Zanjanchi, Photocatalytic self-cleaning properties of cellulose fibers modified by nano-sized zinc oxide, *Thin Solid Films* 519 (2011) 3641–3646.
- [19] I. Perelshtain, G. Applerot, N. Perkas, E. Wehrshetz-Sigl, A. Hasmann, G. Guebitz, A. Gedanken, Antibacterial properties of an in situ generated and simultaneously deposited nanocrystalline ZnO on fabrics, *ACS Appl. Mater. Interfaces* 1 (2009) 361–366.
- [20] G. Applerot, R. Abu-Mukh, A. Irzh, J. Charmet, H. Keppner, E. Laux, G. Guibert, A. Gedanken, Decorating parylene-coated glass with ZnO nanoparticles for antibacterial applications: a comparative study of sonochemical, microwave, and microwave-plasma coating routes, *ACS Appl. Mater. Interfaces* 2 (2010) 1052–1059.
- [21] Y. Xu, M. Schoonen, The absolute energy positions of conduction and valence bands of selected semiconducting minerals, *Am. Miner.* 85 (2000) 543–556.
- [22] H. Yang, L. Mei, P. Wang, J. Generoux, Y. Wang, B. Yi, Ch. Au, L. Dang, P. Feng, Photocatalytic degradation of norfloxacin on different TiO_{2-x} polymorphs under visible light in water, *RSC Adv.* 7 (2017) 45721–45732.
- [23] D. Ding, C. Liu, Y. Ji, Q. Yang, L. Chen, C. Jiang, T. Cai, Mechanism insight of degradation of norfloxacin by magnetite nanoparticles activated persulfate: identification of radicals and degradation pathway, *Chem. Eng.* 308 (2017) 330–339.
- [24] M.M. Haque, M. Muneer, Photodegradation of norfloxacin in aqueous suspensions of titanium dioxide, *J. Hazard. Mater.* 145 (2007) 51–57.
- [25] M. Chen, W. Chu, Degradation of antibiotic norfloxacin in aqueous solution by visible-light-mediated C-TiO₂ photocatalysis, *J. Hazard. Mater.* 219–220 (2012) 183–189.
- [26] M. Chen, W. Chu, H₂O₂ assisted degradation of antibiotic norfloxacin over simulated solar light mediated Bi₂WO₆: kinetics and reaction pathway, *Chem. Eng. J.* 296 (2016) 310–318.
- [27] S. Chen, X. Tang, X. Chen, L. Yingjie, L. Gao, P. Wang, Efficiency and mechanism of photocatalytic oxidation of norfloxacin in wastewater by C/Fe-Bi₂WO₆, *Chin. J. Appl. Chem.* 34 (2017) 936–945.
- [28] V. Santos, M. Meireles, C. Lange, Degradation of antibiotics norfloxacin by fenton, UV and UV/H₂O₂, *J. Environ. Manag.* 154 (2015) 8–12.
- [29] M. Sayed, L.A. Shah, N. Shah, J. Nisar, H. Khan, P. Zhang, A.R. Khan, Efficient photocatalytic degradation of norfloxacin in aqueous media by hydrothermally synthesized immobilized TiO₂/Ti films with exposed {001} facets, *J. Phys. Chem. A* 120 (2016) 9916–9931.
- [30] I. Hassan, S. Sathasivam, S. Nair, C. Carmalt, Antimicrobial properties of copper-doped ZnO coatings under darkness and white light illumination, *ACS Omega* 2 (2017) 4556–4562.
- [31] L. Zhang, R. Dillert, D. Bahnemann, M. Vormoor, Photoinduced hydrophilicity and

self-cleaning: models and reality, *Environ. Sci.* 5 (2012) 7491–7507.

[32] J. Nogier, M. Delamar, P. Ruiz, R. Thampi, P. Albers, J. Kiwi, X-ray photoelectron spectroscopy of TiO_2/V_2O_5 catalysts, *Catal. Today* 20 (1994) 109–123.

[33] John F. Moulder, William F. Stickle, Peter E. Sobol, Kenneth D. Bomben, Jill Chastain (Ed.), *Handbook of X-ray Photoelectron Spectroscopy*, Perkin-Elmer Corporation (Physical Electronics Division), Minnesota, USA, 1992.

[34] D.A. Shirley, High-resolution X-ray photoemission spectrum of the valence bands of gold, *Phys. Rev. B* 5 (1972) 4709–4714.

[35] M.O. Fatehah, A.A. Hamidi, S. Stoll, Stability of ZnO nanoparticles in solution, influence of pH, dissolution, aggregation and disaggregation effects, *J. Colloid Sci. Biotechnol.* 3 (2014) 1–10.

[36] J. Tauc, Optical properties and electronic structure of amorphous Ge and Si, *Mater. Res. Bull.* 3 (1968) 37–46.

[37] B. Sulzberger, S. Canonica, T. Egli, W. Giger, J. Klausen, U. von Gunten, Oxidative transformations of contaminants in natural and in technical systems, *Chimia* 51 (1997) 900–907 and references therein.

[38] H. Bouyarmane, I. El Hambalali, M. El Karbani, A. Rami, A. Saoiabi, S. Saoiabi, S. Masse, T. Coradin, A. Laghzitil, Parameters influencing ciprofloxacin, ofloxacin, amoxicillin and sulfamethoxazole retention by natural and converted calcium phosphates, *J. Hazard. Mater.* 30 (2015) 38–44 and references therein.

[39] G.A. Parks, The isoelectric points of solid oxides, solid hydroxides, and aqueous hydroxo complex systems, *Chem. Rev.* 65 (1965) 177–198.

[40] A. Fujishima, X. Zhang, D. Tryk, TiO_2 photocatalysis and related surface phenomena, *Surf. Sci. Rep.* 63 (2008) 515–582.

[41] G. Mamba, C. Pulgarin, M. Bensimon, J. Kiwi, S. Rtimi, Synchronic coupling of $Cu_2O(p)/CuO(n)$ semiconductors leading to norfloxacin degradation under visible light: kinetics, mechanism and film surface properties, *J. Catal.* 353 (2017) 133–140.

[42] Z. Kang, X. Yan, Y. Wang, Z. Bai, Y. Liu, Z. Zhang, P. Lin, X. Zhang, H. Yuan, X. Zhang, Y. Zhang, Electronic structure engineering of Cu_2O film/ZnO nanorods array all-oxide p-n heterostructure for enhanced photo-electrochemical property and self-powered bio-sensing application, *Sci. Rep.* 5 (2015) 7882–7887.

[43] P. Lin, X. Chen, X. Yan, Z. Zhang, H. Yuan, P. Li, Y. Zhao, Y. Zhang, Enhanced photo-response of Cu_2O/ZnO hetero-junction with piezo-modulated interface engineering, *Nano Res.* 7 (2014) 860–868.

[44] Q. Simon, D. Berreca, A. Gasparotto, C. Maccato, E. Tondello, C. Sada, E. Comini, G. Sberveglieri, M. Banerjee, K. Xu, A. Devi, R.A. Fischer, CuO/ZnO nanocomposite gas sensors develop by a plasma-assisted route, *ChemPhysChem* 13 (2012) 2342–2348.

[45] Paolo Dolcet, Maurizio Casarin, Chiara Maccato, Laura Bovo, Gloria Ischia, Stefano Gialanella, Fabrizio Mancin, Eugenio Tondello, Silvia Gross, Miniemulsions as chemical nanoreactors for the room temperature synthesis of inorganic crystalline nanostructures: ZnO colloids, *J. Mater. Chem.* 22 (2012) 1620–1626.

[46] Z. He, Y. Xia, B. Tang, X. Jiang, J. Su, Fabrication of photocatalytic property of ZnO/ Cu_2O core-shell nanocomposites, *Mater. Lett.* 184 (2016) 148–151.

[47] A.E. Kandjani, Y.M. Sabri, S.R. Periasamy, N. Zahora, M.H. Amin, A. Nafady, S.K. Bhargava, Controlling core/shell formation of nano-cubic p- $Cu_2O/n-ZnO$ toward enhanced photocatalytic performance, *Langmuir* 31 (2015) 10922–10930.

[48] W. Wan, L. Zhu, L. Hu, G. Chen, W. Mi, Z. Ye, Investigation of the morphology evolution of Cu-ZnO nanorod arrays and enhancement of ferromagnetism by co-doping with N, *Phys. Lett. A* 378 (2014) 2763–2767.

[49] H. Xue, Y. Chen, X.L. Lu, G.H. Zhang, H. Zhang, S.Y. Ma, X-ray diffraction spectroscopy and X-ray photoelectron spectroscopy studies of Cu-doped ZnO-films, *Phys. E: Low-Dimens. Syst. Nanostruct.* 41 (2009) 788–791.

[50] A. Shirzadi, A. Nezamzadeh-Ejhieh, Enhanced photocatalytic acidity of supported CuO-ZnO smiconductors towards the photo-degradation of mefenamic acid aqueous solution as a real sample, *J. Mol. Catal. A* 411 (2016) 222–229.